Modulation of alpha oscillations by attention is predicted by hemispheric asymmetry of subcortical regions.

Tara Ghafari[1], Cecilia Mazzetti[1], Kelly Garner[2], Tjerk Gutteling[1,3], Ole Jensen[1]

[1]Centre for Human Brain Health, School of Psychology, University of Birmingham, UK; [2]School of Psychology, University of New South Wales, Australia. [3]CERMEP-Imagerie du Vivant, MEG Department, Lyon, France

Abstract

Evidence suggests that subcortical structures play a role in high-level cognitive functions such as the allocation of spatial attention. While there is abundant evidence in humans for posterior alpha band oscillations being modulated by spatial attention, little is known about how subcortical regions contribute to these oscillatory modulations, particularly under varying conditions of cognitive challenge. In this study, we combined MEG and structural MRI data to investigate the role of subcortical structures in controlling the allocation of attentional resources by employing a cued spatial attention paradigm with varying levels of perceptual load. We asked whether hemispheric lateralization of volumetric measures of the thalamus and basal ganglia predicted the hemispheric modulation of alpha-band power. Lateral asymmetry of the globus pallidus, caudate nucleus, and thalamus predicted attention-related modulations of posterior alpha oscillations. When the perceptual load was applied to the target and the distractor was salient caudate nucleus asymmetry predicted alpha-band modulations. Globus Pallidus was predictive of alpha-band modulations when either the target had a high load, or the distractor was salient, but not both. Finally, the asymmetry of the thalamus predicted alpha band modulation when neither component of the task was perceptually demanding. In addition to delivering new insight into the subcortical circuity controlling alpha oscillations with spatial attention, our finding might also have clinical applications. We provide a framework that could

be followed for detecting how structural changes in subcortical regions that are associated with neurological disorders can be reflected in the modulation of oscillatory brain activity.

Introduction

The visual world provides more sensory information than we can be aware of at any given moment. Thus, our brains must prioritise goal-relevant over distracting information. A rich body of research shows that the brain amplifies goal-relevant inputs, and suppresses non-relevant inputs by a process referred to as selective attention (1–3). There is ample evidence for top-down control of neocortical regions associated with sensory processing when information is prioritized (1,4,5). The dorsal attention network, which consists of the intraparietal sulcus/superior parietal lobule, and the frontal eye fields, is the most predominant network associated with the allocation of attention (6–8). However, although the role of neocortex for spatial attention and cognitive control has been extensively studied, the contributions of subcortical regions are less well understood. One reason, amongst many others, is that MEG and EEG are not well suited for detecting subcortical activity. Therefore, the present study aims to provide insights into the contribution of the thalamus and basal ganglia in driving top-down spatial attention.

There has been intense focus on the cortical contributions to the top-down control processes, yet there are multiple sources of evidence to suggest that subcortical structures also play an important role in cognitive control. For instance, it has been shown that the pulvinar plays an important role in the modulation of neocortical alpha oscillations associated with the allocation of attention (9). Studies in rats and non-human primates have shown that both the thalamus and superior colliculus, are involved in the control of spatial attention by contributing to the regulation of neocortical activity (9–11). Notably, when the largest nucleus of the thalamus, the pulvinar, was inactivated after muscimol infusion, the monkey's ability to detect colour changes in attended stimuli was lowered. This behavioral deficit occurred when the target was in the receptive field of V4 neurons that were connected to lesioned pulvinar (12). The basal ganglia play a role in different aspects of cognitive control, encompassing attention (13,14),

behavioural output (15), and conscious perception (16). Moreover, the basal ganglia contribute to visuospatial attention by linking with cortical regions like the prefrontal cortex via the thalamus. . Anatomical tracing studies on selective attention and distractor suppression point to a key role of prefrontal-basal ganglia-thalamus pathway whereby sensory thalamic activity is regulated by prefrontal cortex via basal ganglia (14). Furthermore, fMRI studies in humans demonstrated increased activation in basal ganglia when covert attention was reallocated. Additionally, dynamic causal modelling has shown that the basal ganglia can modulate the top-down influence of the prefrontal cortex on the visual cortex in a task-dependent manner (17).

In terms of neuronal dynamics, power modulation of oscillatory activity in the alpha band (8-13Hz) has been proposed to reflect resource allocation between goal-relevant and irrelevant stimuli. This has consistently been shown between studies in EEG and MEG in which attention is allocated to the left or right hemifield. Such studies typically find an alpha power decrease in the hemisphere contralateral to the attended stimuli complemented by a relative increase in alpha power in the other hemisphere associated with unattended stimuli (Okazaki et al., 2014; Thut et al., 2006; Worden et al., 2000). It is debated whether the alpha power associated with the unattended stimuli is under task-driven top-down control or rather explained by an indirect control mechanism driven by the engagement of the target (22). The latter notion is aligned with perception load theory that is defined as the perceptual demand of the task or relevant stimulus, according to which the (finite) resources are allocated (23). Indeed, a recent study demonstrated when the target stimulus has a higher perceptual load (e.g., more difficult to perceive), alpha band power increases in ipsilateral regions thus indirectly reflecting distractor suppression (24).

Based on these findings, both oscillatory activity in the alpha band and the activity of subcortical structures are involved in the allocation of attentional resources. The direct relationship between activity in subcortical regions and neocortical oscillations is poorly understood in humans, in part owing to the difficulty in detecting the activity of deep structures using MEG/EEG. One way around this is to instead investigate, the relationship between the volumetric measures of subcortical structures and oscillatory brain activity by combining MRI

and electrophysiological measures such as MEG. Using this approach, it was shown that the hemispheric lateralized modulation of alpha oscillations is correlated with the volumetric hemispheric asymmetry of both the globus pallidus and the thalamus (25). The relationship between the globus pallidus and the modulation of alpha oscillations was demonstrated in the trials where the visual stimuli were associated with high-value (positive or negative) reward valence.

In this study, we aimed to identify a link between the volumetric asymmetries of subcortical structures and the modulation of alpha oscillations in the context of spatial attention without explicit reward-associations. Given the assumed contribution of the basal ganglia to reward-based learning (26–29), it is perhaps unsurprising to find contributions of the globus pallidus in the paradigms targeting reward valence. What remains to be determined is whether these structures play a more general role in the formation of spatial attention biases. We analyzed MEG and structural data from a previous study (24), in which spatial cues guided participants to covertly attend to one stimulus (target) and ignore the other (distractor). To investigate the relationship between the allocation of attentional resources and mechanisms of neural excitability and suppression., the target load and the visual saliency of the distractor were manipulated using a noise mask. This load/salience manipulation resulted in four conditions that affect the attentional demands of target and distractor. We utilized the hemispheric laterality of subcortical structures and alpha modulation to overcome issues related to individual variations in oscillatory power and head-size. This approach allowed us to relate the hemispheric volumetric asymmetries in thalamus, caudate nucleus, and globus pallidus to the modulation of alpha oscillations when spatial attention is allocated under varying conditions of cognitive challenge. By examining their role in a task without explicit reward, we aim to elucidate the generalizability of the contributions of subcortical structures to spatial attention modulation. Such a finding would implicate a role for the basal ganglia in cognition beyond the well-studied realm of the estimation of choice values (30). Specifically, in a prior study (25), we observed that the contributions of the basal ganglia were most pronounced when the items in question were associated with a reward. Our current findings broaden our understanding of

how subcortical structures are involved in modulating alpha oscillations during top-down spatial attention, in the absence of any reward or value associations.

Results

We investigated the relationship between the volumetric lateralization of subcortical structures estimated from structural MRIs and the hemispheric modulation of alpha oscillations measured by MEG in a spatially cued change detection task. We asked the participants to covertly attend to face-stimuli in the left or right visual field and indicate the direction of a subtle gaze-shift of the attended face (Figure 1A). The influences of perceptual load and distractor salience were examined by combining noisy and clear target and distractor stimuli in a 2 x 2 design (Figure 1B).

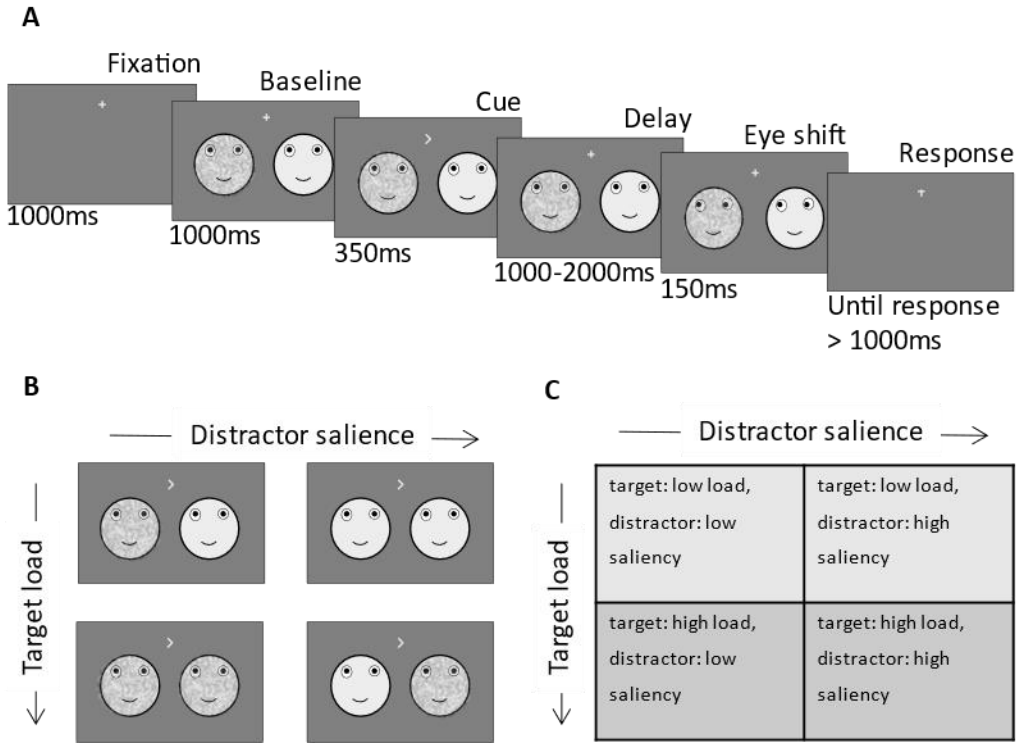

Figure 1. Schematic of experimental design. A. Two face stimuli were presented simultaneously in the left and right hemifield. After baseline, a directional cue indicated the location of the

target. After a variable delay interval (1000-2000ms) the eye-gaze of each stimulus (independent of the other) shifted randomly to the right or left. Subjects had to indicate the direction of the target eye movement after the delay interval. B. Examples of visual stimuli for each of the four conditions C. Table with the labels of the four load/salience conditions.

Modulation of alpha power with respect to left and right cues

To quantify the anticipatory change in alpha power, we analysed the modulation of power in the -850 – 0 ms interval prior to the target. As expected from a previous report (24), we observed a power decrease contralateral to the cued hemifield and a relative increase ipsilaterally (i.e. an increase contralateral to the distractor, Figure 2A) As expected, the magnitude of the modulation index (MI(α)) reflecting the relative difference in alpha power when attending left versus right, gradually decreased and increased over respectively the left and right hemisphere until target onset (Figure 2B). We then identified symmetric clusters of sensors (5 over each hemisphere) that showed the highest modulation of alpha power (Figure 2C) and focused the subsequent analyses on these sensors of interest.

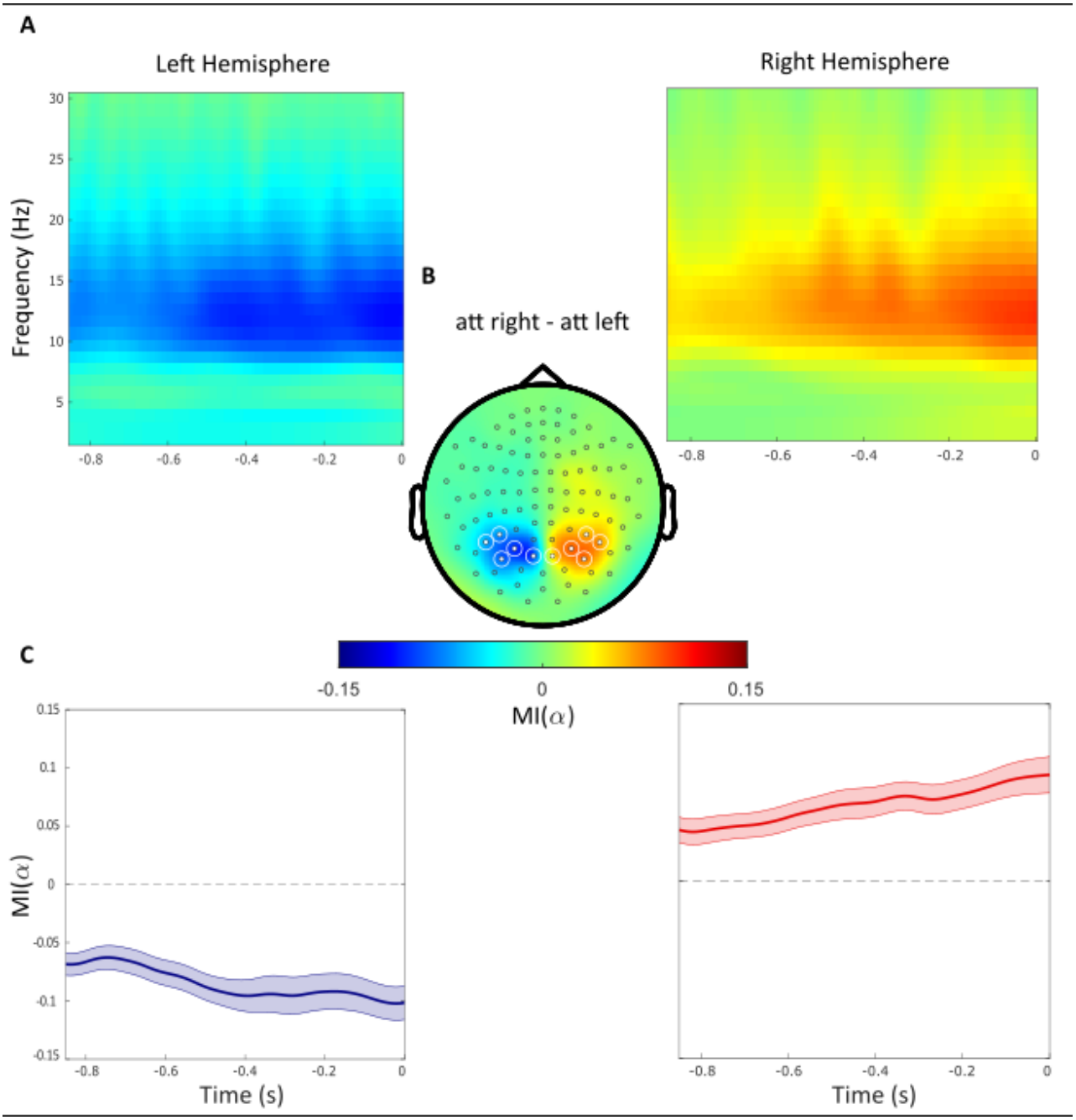

Figure 2. Alpha power decreases contralaterally and increases ipsilaterally with respect to the cued hemifield. A. Time-frequency representations of power demonstrate the difference between attended right versus left trials (t = 0 indicate the target onset). B. Topographical plot of the relative difference between attend right versus left trials. Regions of Interest sensors

(ROIs) are marked with white circles. C. The alpha band modulation (MI(α)) averaged over ROI sensors within the left and right hemispheres, respectively. The absolute MI(α) increased gradually during the delay interval until the onset of the target stimuli.

Hemispheric asymmetry of subcortical regions

Next, we computed the hemispheric lateralization modulation of alpha power (HLM(α)) in each individual. We did so using the HLM(α) index which quantifies how strongly the alpha power in the left hemisphere is modulated by attention with respect to alpha power modulations in the right hemisphere.

The histogram in figure 3A illustrates the distribution of HLM(α) in all participants. HLM(α) indices range from ~-0.15 to 0.15 and are normally distributed around zero before target onset (Shapiro-Wilk, W = 0.966, p-value = 0.3895).

We then calculated the hemispheric lateralized volumes of the seven subcortical structures, as illustrated in Figure 3B (thalamus, caudate nucleus, putamen, globus pallidus, hippocampus, amygdala, and nucleus accumbens) using the FIRST algorithm on the MRI data. Thalamus (mean ± std = -0.0123 ± 0.0121, p-value < 0.000), putamen (mean ± std = -0.0149 ± 0.0285, p-value = 0.004) and nucleus accumbens (mean ± std = -0.1141 ± 0.0746, p-value < 0.000) have significantly negative LV values (i.e., left lateralization) whereas the caudate nucleus is right lateralized (mean ± std = 0.0115 ± 0.0285, p-value = 0.021) (Figure 3B). Globus pallidus, hippocampus, and amygdala did not show any robust volume lateralization.

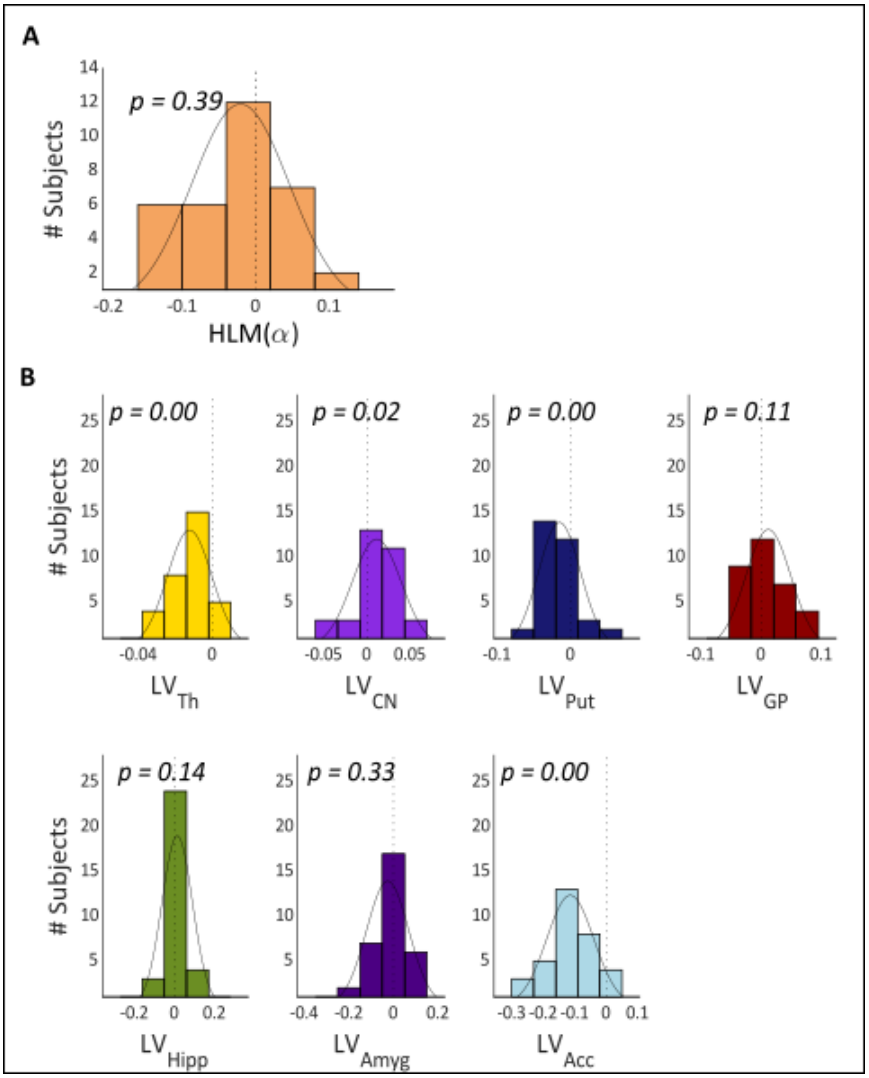

Figure 3. Hemispheric lateralization modulation (HLM(a)) grand average and basal ganglia volumes across all participants. A, The HLM(a) distribution across participants. While there was considerable variation across participants, we observed no hemispheric bias in lateralized modulation values across participants (p-value = 0.39). B, Histograms of the lateralization volumes of subcortical regions. We found that caudate nucleus was right lateralized (p-value = 0.021) whereas, putamen, nucleus accumbens and thalamus volumes showed left lateralization (p-value = 0.004, p-value < 0.001 and p-value < 0.001, respectively). Th = Thalamus, CN = Caudate nucleus, Put = Putamen, GP = Globus Pallidus, Hipp = Hippocampus, Amyg = Amygdala, Acc = Nucleus Accumbens.

Relationship between subcortical regions and hemispheric alpha lateralization

To test whether the individual hemispheric asymmetries in subcortical grey matter relate to variability in HLM(α), we subjected the MEG and MRI data to a General Linear Model (GLM). In this model, the individual HLM(α) values was the dependent variable, and the individual hemispheric lateralization volumes (LV) of the subcortical region were the explanatory variables. To discover the best set of subcortical structures that predict HLM(α) we used all possible combinations of regressors (LV) and selected the winning model based on lowest Akaike Information Criterion (AIC) scores. The winning model constituted of thalamus, caudate nucleus and globus pallidus and is defined as:

$$HLM(\alpha) \sim \beta_0 + \beta_1 LV_{Th} + \beta_2 LV_{CN} + \beta_3 LV_{GP} + \varepsilon$$

Where HLM(a) indicates the hemispheric lateralization modulation of alpha power and LV_{Th}, LV_{CN}, LV_{GP} refer to the lateralization volumes of thalamus, caudate nucleus and globus pallidus, respectively.

The analysis showed that the participants with larger volumes of the caudate nucleus in the left compared to the right hemisphere showed higher modulations in alpha power over the left compared to the right hemisphere (and vice versa). There was a trend for the same effect for the globus pallidus whereas the thalamus shows the opposite effect. These results were observed from the winning model that contained LV_{Th}, (beta = -2.19, $T_{(29)}$ = -2.74, se = 0.80, p = 0.010), LV_{CN} (beta = 0.92, $T_{(29)}$ = 2.83, se = 0.33, p-value = 0.008) and LV_{GP} (beta = 0.51, $T_{(29)}$ = 1.95, se = 0.26, p-value = 0.061) as regressors. This model predicted the HLM(α) values significantly in the GLM ($F_{3,29}$ = 7.4824, p = 0.0007, adjusted R^2 = 0.376) as compared with an intercept-only null model (Figure 4A). These findings are illustrated in Figure 4B, confirming that both thalamus and caudate nucleus showed a significant linear partial regression with hemispheric lateralization modulation in the alpha band in the opposite and same direction.

198 Although, the beta estimate of LV_{GP} only showed a positive trend, removing it from the
199 regression resulted in worse models (AIC and BIC tables in supplementary material).

200

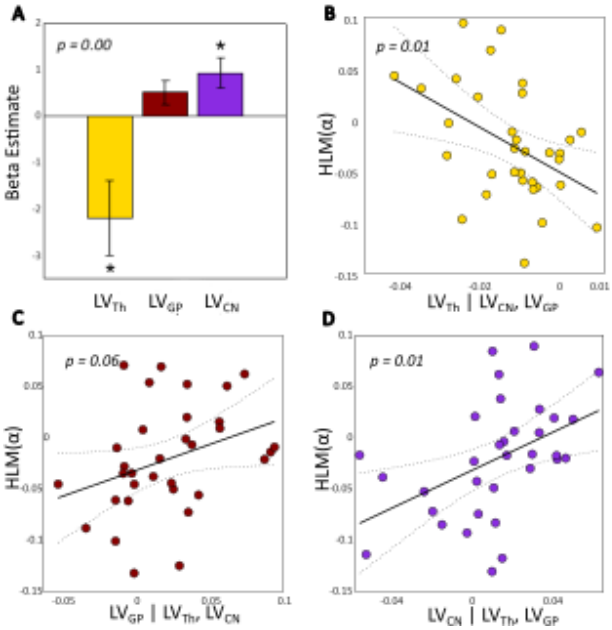

201

202 Figure 4. Lateralization volume of thalamus, caudate nucleus and globus pallidus in relation to
203 hemispheric lateralization modulation of alpha (HLM(α)) in the task. A, The beta coefficients for
204 the best model (containing three regressors) associated with a generalized linear model (GLM)
205 where lateralization volume (LV) values were defined as explanatory variables for HLM(α). The
206 model significantly explained the HLM(α) (p-value = 0.0007). Error bars indicate standard errors
207 of mean (SEM). Asterisks denote statistical significance; *p<0.05. B, Partial regression plot
208 showing the association between LV_{Th} and HLM(α) while controlling for LV_{GP} and LV_{CN} (p-value
209 = 0.01). C, Partial regression plot showing the association between LV_{GP} and HLM(α) while
210 controlling for LV_{Th} and LV_{CN} (p-value = 0.061) . D, Partial regression plot showing the
211 association between LV_{CN} and HLM(α) while controlling for LV_{Th} and LV_{GP} (p-value = 0.008).
212 Negative (or positive) LVs indices denote greater left (or right) volume for a given substructure;
213 similarly negative HLM(α) values indicate stronger modulation of alpha power in the left

compared with the right hemisphere, and vice versa. The dotted curves in B, C, and D indicate 95% confidence bounds for the regression line fitted on the plot in red.

It is worth noting that neither the behavioural nor the rapid invisible frequency tagging (RIFT) measures showed significant relationships with LVs and HLM(α) (Supplementary material, Figure 1 and Table 3).

Association between volumetric lateralization of subcortical regions and attention related to perceptual load conditions.

To relate load and salience conditions of the task to the relationship between subcortical structures and the alpha activity, we combined low-load or high-load targets with high-saliency or low-saliency distractors to manipulate the perceptual load appointed to each trial (Method section, Figure 1).

We therefore applied a multivariate multiple regression (MMR) using the HLM(α) values from each load/salience condition, and the LV values of the thalamus, caudate nucleus and globus pallidus (Equation 5). Comparison of the full (i.e., MMR including the LV values of all seven subcortical structures as regressors) and reduced (i.e., MMR with all structures excluding the selected structures) models showed that our selected regressors predicted variability in HLM(α) values to an extent that was greater than chance ($F_{(25,28)}$ = 2.03, p-value = 0.037). This was further confirmed when we compared the MMR model with the null model (i.e., MMR including only subject intercepts as regressor) ($F_{(29,31)}$ = 3.78, p-value = 0.0015). We next examined the extent to which LV values from each subcortical region predicted HLM(α) values for each load/salience condition. Our analysis, as shown in Figure 5, demonstrated that the thalamus had significant LV values in condition 1 (i.e., low-load target, non-salient distractor) with beta = -3.63 ($T_{(29)}$ = -2.64, se = 1.37, p-value = 0.0132). Globus pallidus showed a significant beta coefficient in conditions 2 (i.e., high-load target, non-salient distractor) and 3 (i.e., low-load target, salient distractor) with beta = 0.93, ($T_{(29)}$ = 2.15, se = 0.43, p-value = 0.040) and beta = 0.89 ($T_{(29)}$ = 2.30, se = 0.39, p-value = 0.029), respectively. Condition 4 (i.e., high-load target, salient distractor) was the only condition in which the caudate nucleus had a beta estimate

241 significantly different than zero (beta = 1.64, $T_{(29)}$ = 2.07, se = 0.79, p-value = 0.049). To
242 ascertain whether each predictor contributes to all conditions, we conducted statistical tests on
243 the results of our MMR, testing the null hypothesis that a given regressor does not impact all
244 dependent variables. We found that while, with marginal significancy, caudate nucleus can
245 predict variability across all four of the task conditions ($F_{(26,4)}$ = 2.82, p-value = 0.046), the
246 predictive relationships of thalamus ($F_{(26,4)}$ = 2.43, p-value = 0.073) with condition 1, and globus
247 pallidus ($F_{(26,4)}$ = 2.29, p-value = 0.087) with conditions 2 and 3 hold only for these conditions. In
248 sum, this demonstrates that when the task is easiest (condition 1), the thalamus is related to
249 alpha modulation. When the task is most difficult (condition 4), the caudate nucleus relates to
250 the alpha modulation, however, its contributions are substantial enough to predict outcomes
251 across all conditions. For the conditions with medium difficulty (conditions 2 and 3) the globus
252 pallidus is related to the alpha band modulation.

253

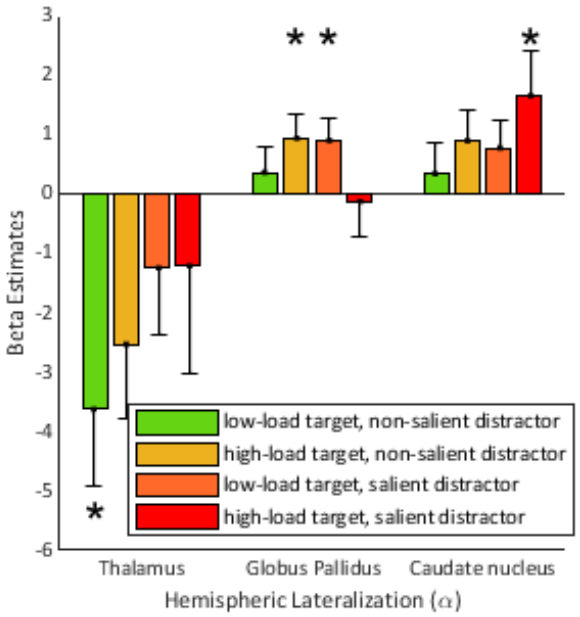

254

255 Figure 5. Beta estimates of subcortical nuclei from a multivariate regression model predicting
256 HLM(α) in the four perceptual load conditions. Here the HLM(α) values for the four load
257 conditions are the dependent variables and the lateralization volume of subcortical structures

are the explanatory variables. The model significantly explains HLM(α) variability (p-value = 0.001) in comparison with null model). Error bars indicate SEM. Asterisks denote statistical significance; *p-value < 0.05.

Discussion

In the current study, we sought to identify the association between the volumetric hemispheric asymmetries in subcortical structures and the hemispheric laterality in the modulation of posterior alpha oscillations during varying conditions of perceptual load. This association was tested in the context of a spatial attention paradigm where target load and distractor salience were manipulated. Our study resulted in two main findings: 1) globus pallidus, caudate nucleus, and thalamus predicted attention-related modulations of posterior alpha oscillations. 2) Each of these subcortical structures contributed differently to the lateralization values associated with the perceptual load conditions. For the easier task condition, the thalamus showed strong predictive power for alpha power modulation, whereas for mid-levels of load and salience, the globus pallidus showed predictive value. For the most perceptual demanding condition, we found that asymmetry of the caudate nucleus predicted alpha power modulation. These results shed light on the role of subcortical structures and their involvement in the modulation of oscillatory activity during the allocation of spatial attention.

Thalamus, Caudate nucleus, and Globus Pallidus are involved in the allocation of spatial attention.

While some MEG studies have demonstrated that it is possible to detect activity from deep structures such as the hippocampus (31–34), it is questionable whether one in general can use MEG to reliably detect activity from the thalamus and basal ganglia, owing to low SNR from sources close to the centre of the head (Baillet, 2017). Given these constraints, we instead correlated MEG data with structural magnetic resonance images to uncover functional contributions of subcortical structures to spatial attention.

283 We evaluated the relationship between subcortical structures and cortical oscillatory activity
284 relying on the association between structure and function. Previous research points to a link
285 between the volume of a given brain region and its functionality. It has been demonstrated that
286 extensive navigation experience enlarges the size of right hippocampus (37). Furthermore, in
287 terms of neurological disorders, it is well established that shrinkage (atrophy) in specific regions
288 is a predictor of a number of neurological and psychiatric conditions including Parkinson's
289 disease, dementia, and Huntington's disease. In Parkinson's disease, atrophy in the nucleus
290 accumbens and thalamus correlated with cognitive impairments (38). In a large-scale study on
291 773 participants, patients with Alzheimer's Disease have been shown to have a significantly
292 smaller amygdala, thalamus, caudate nucleus, putamen, and nucleus accumbens than matched
293 controls (39). It has also been shown that the spatial extent of pathological change in
294 subcortical structures can predict cognitive changes in Parkinson's Disease (40). Patients with
295 symptomatic Huntington's Disease also show significantly smaller caudate nucleus than pre-
296 symptomatic participants who were carriers of Huntington's Disease gene mutation (41).
297 Changes in neocortical oscillatory activity have also been observed in neurological disorders
298 which mainly are known to affect subcortical structures. For example, individuals with
299 Alzheimer's Disease demonstrate an increase in slow oscillatory activities and a decrease in
300 higher frequency oscillations (42). Moreover, in patients with Parkinson's Disease, the power of
301 beta oscillations increases relatively to when they are dopamine-depleted compared with when
302 they are on dopaminergic medication (43).

303 Based on these considerations, we argue that the volume of basal ganglia relates to the ability
304 to modulate posterior brain oscillations in attention type tasks. We demonstrated this by
305 considering the hemispheric lateralization of the basal ganglia structures in relation to the
306 ability to modulate posterior alpha oscillations. Employing hemispheric lateralization was
307 motivated by the organizational characteristic of structural asymmetry in healthy brain (44).
308 Additionally, considering the effects of aging (45) and neurodegenerative disorders, such as
309 Alzheimer's Disease (46), on brain symmetry influenced this approach.. Furthermore,
310 computing lateralization indices for individuals addresses the challenge of accommodating

variations in both head size and the power of oscillatory activity. . Our findings are consistent with previous studies suggesting that thalamic and basal ganglia structures are involved in modulating oscillatory activity in the alpha band. For example, the largest nucleus of the thalamus, the pulvinar, supports the allocation of spatial attention by driving the oscillatory synchrony in the alpha band between cortical areas in a task-dependent manner (47) Also, our finding are consistent with other studies suggestions a role for the caudate nucleus (48) and the pulvinar when allocating spatial attention (48–50). Stimulation of the subthalamic nucleus has been shown to suppress oscillatory activity in the alpha and beta (8-22Hz) frequency bands (51). Furthermore, our regression analysis outcomes align with the findings of Mazzetti et al. (25) underscoring the significant predictive influence exerted by the lateralized volume of globus pallidus on the modulation of hemispheric lateralization in alpha oscillations during spatial attention tasks. This convergence of results not only corroborates the validity and consistency of our findings but also extends the empirical foundation supporting the predictive role of the asymmetry of globus pallidus in modulating alpha oscillations beyond reward valence and to the context of attention.

Thalamus, Globus Pallidus, and Caudate nucleus play varying roles across different load conditions.

Our results demonstrate a shift in the contribution of the thalamus, globus pallidus, and caudate nucleus when increasing the perceptual load of the target and saliency of the distractor. While in the low load, low saliency condition, the lateralized volume of the thalamus was correlated with the interhemispheric bias in alpha modulation, in the low load, high saliency, as well as high load, low saliency conditions, globus pallidus was related to the alpha oscillatory activity. Finally, the caudate nucleus was mainly associated with the high load, high saliency condition.

This differing pattern of the thalamic and basal ganglia structures might be suggestive of their respective contributions to the control of attentional resources. Involvement of the thalamus when the task is in its simplest form can be explained by its role relaying information between

338 the basal ganglia and the prefrontal cortex (52,53). The opposite effect of the globus pallidus
339 compared to the thalamus is striking, and possibly explained by the globus pallidus containing
340 GABAergic interneurons. Thus the inhibitory nature of the globus pallidus projections to
341 thalamus could explain why they are related to the alpha modulation in different manners (54).
342 The involvement of the caudate nucleus in the most difficult condition is also in line with
343 previous findings showing activation of caudate nucleus only in the higher-level cognitive
344 hierarchy in a working memory selection (55) as well as a language task (53). The engagement
345 of globus pallidus might be reflected from its central role in harmonizing firing rates across the
346 cortico-basal-ganglia circuits (56). Globus pallidus also has wide projections to the thalamus
347 (57) and can thereby impact the dorsal attentional networks by modulating prefrontal activities
348 (14). Although these findings highlight the varying contributions of different regions, they do
349 not imply a lack of evidence for correlations between these subcortical structures and other
350 load conditions.

351 *Limitations and future directions*

352 In the current study, we correlated the volumetric asymmetry of subcortical structures with the
353 lateralized power of alpha oscillation. While this method provides novel insights into the role of
354 subcortical structures in the modulation of oscillatory activity, it is indirect. The association
355 between the function of subcortical nuclei and cortical oscillatory activity needs to be
356 investigated further in electrophysiological studies that record the activity of both regions
357 simultaneously. This could be done in non-human primates or in humans implanted with
358 electrodes in the globus pallidus in treatment for Parkinson's Disease. In particular, EEG paired
359 with globus pallidus recordings in participants performing spatial attention tasks would be of
360 great value. Furthermore, in this study, our emphasis has been on assessing the size of
361 subcortical structures. Future investigations could explore subcortical white matter
362 connectivities and hemispheric asymmetries. This approach has previously been conducted on
363 superior longitudinal fasciculus (SLF) (58,59) and holds potential for examining cortico-
364 subcortical connectivity in the context of oscillatory asymmetries.

365 Moreover, the current study faced methodological constraints, limiting the analysis to the
366 entire thalamus. Additionally, we refrained from directly comparing the contributions of
367 subcortical structures to different conditions due to low statistical power. It would be of great
368 interest to conduct further investigations to quantify the distinct impacts of individual thalamic
369 nuclei on the association between subcortical structures and the modulation of oscillatory
370 activity. In future studies it would be interesting to design an experiment directly addressing
371 which subcortical regions contribute to distractor and target load in terms of modulating the
372 alpha band activity. In order to ensure sufficient statistical power for doing so possibly each
373 factor needs to be addressed in different experiments.

374 Moreover, our failure to identify a relationship between the lateralized volume of subcortical
375 structures and behavioural measures should be addressed in studies that are better designed to
376 capture performance asymmetries (60). Individual preferences toward one hemifield, which
377 were not addressed in the current study design, could potentially strengthen the power to
378 detect correlations between structural variations in the subcortical structures and behavioural
379 measures. For example, it would be of great significance to investigate the lateralization of
380 subcortical structures in patients with hemineglect in relation to right hemisphere lesions (61).

381 We did not find any association between the power of RIFT signal and the size asymmetry of
382 subcortical structures. Since Bayes factors were less than 0.1, we conclude that our RIFT null
383 findings are robust, suggesting a dissociation between how alpha oscillations and neuronal
384 excitability indexed by RIFT relate to subcortical structures. In previous work we have
385 demonstrated that the attention modulation of the RIFT signal is strongest observed in early
386 visual cortex, whereas alpha oscillations are more strongly modulated around the parieto-
387 occipital sulcus (62). It has been proposed that the modulation in RIFT in early visual cortex with
388 attention reflects gain control. According to this framework, we conclude that subcortical
389 regions might not be involved in gain modulation in early visual cortex during the allocation of
390 spatial attention, but rather in the downstream gating of visual information.

Conclusion

Our findings point to a link between thalamus and nuclei of the basal ganglia and measures of alpha oscillations in relation to spatial attention. Moreover, they demonstrate distinguished contributions of the different subcortical structures depending on target load or distractor salience, thus informing theories of how subcortical structures relate to oscillatory dynamics in challenging attentional settings. The stage is now set for further investigating the relationship between subcortical regions and the modulation of oscillatory activity. Linking brain oscillations to changes in subcortical regions associated with neurological disorders, such as Alzheimer's Disease (39,63) and Parkinson's Disease (Mak et al., 2014), could have potential clinical applications in terms of early diagnosis. Our approach could also be extended to other tasks resulting in hemispheric lateralization of oscillatory brain activity, e.g. working memory tasks (64) or language tasks (65). Our results also call for more direct investigations of the relationship between subcortical regions and neocortical oscillations which is best done by intracranial recordings in non-human primates or utilizing human recording from deep-brain stimulation electrodes combined with EEG or MEG.

Methods and Materials

Participants

We analysed a previously collected dataset, described in (24). 35 right-handed healthy volunteers (25 female, mean age: 24 $\pm$ 5.7) participated. All reported normal or corrected-to-normal vision. One participant did not give consent for their data to be used outside of the original study and one was removed due to poor MRI [segmentation] quality, resulting in 33 participants in total. All subjects signed an informed consent form before participation and were paid £15 per hour. The study was conducted in compliance with the Declaration of Helsinki and was approved by the Science, Technology, Engineering, and Mathematics (STEM) ethical review committee of the University of Birmingham.

Experimental design

Participants were instructed to perform a cued change detection task (2 blocks of 256 trials, 45 minutes; Fig 1A), designed to assess selective attention function under varying conditions of perceptual challenge. Each trial started with a fixation point (1000ms) followed by two faces presented on the left and right side of the screen (1000ms). The fixation cross then turned into an arrowhead for 350ms cueing the left or the right hemifield. After a variable 1000 to 2000ms delay, the eye-gaze of each face randomly shifted rightward or leftward in a 150 ms interval. Then followed a 1000 ms response interval where participants were asked to respond with their right or left index finger whether the gaze direction of the cued face shifted left or right (NAtA technologies, Coquitlam, BC, Canada). The experimental paradigm was implemented on a Windows 10 computer running MATLAB (Mathworks Inc., Natrick, USA) using Psychophysics Toolbox 3.0.11 (66,67).

Visual stimuli

Stimuli were circular faces that comprised 8˚ visual angle in diameter and placed with 7˚ eccentricity from fixation and were presented in the lower hemifield. Over trials, the perceptual load of targets was manipulated using a noise mask; noisy targets are harder to detect than clear targets and therefore incur greater perceptual load in their detection. The saliency of distractor stimuli was also manipulated using a noise mask; noisy distractor stimuli are less salient than clear distractors and therefore less disruptive to performance on the detection task. The noise mask was created by randomly swapping 50% of the stimulus pixels (Figure 1B). This manipulation resulted in four target-load/distractor-saliency conditions: (1) target: low load, distractor: low saliency (i.e., clear target, noisy distractor), (2) target: high load, distractor: low saliency (i.e., noisy target, noisy distractor), (3) target: low load, distractor: high saliency (i.e., clear target, clear distractor), (4) target: high load, distractor: high saliency (i.e., noisy target, clear distractor) (Figure 1B and C). The stimulus set consisted of eight different face identities that were randomized across trials. On each trial, the identities of both stimuli were

the same; however, to avoid visual differences between left and right the faces were mirror symmetric from the fixation point. Stimuli were projected using a VPixx PROPixx projector (VPixx technologies, Saint-Bruno, Canada) in Quad RGB mode (1440Hz) with an effective resolution of 960x540 pixels. Face stimuli were tagged with an invisible rapid-frequency-tagged flicker (for more details please refer to Gutteling et al., 2022). The distance between the participant and the projection screen was 148cm resulting in a 25.6˚ of visual angle screen.

Structural data acquisition

T1-weighted magnetic resonance images were acquired for 10 participants on a 3 Tesla Magnetom Prisma whole-body scanner (Siemens AG) with acquisition parameters: TR/TE = 2000/2.01 ms, TI = 880 ms, FoV = 256×256×208 mm^3, acquired voxel size = 1x1x1 mm^3. For 23 participants MRI images were attained from previous studies. These scans were obtained at the former Birmingham University Imaging Center (3-Tesla Philips Achieva Scanner: TR/TE = 7.4/3.5 ms, FA = 7°, FOV = 256x256x176 mm^3, acquired voxel size = 1x1x1 mm^3) were used. The 2 remaining participants provided their MRIs from other sources.

Structural data analysis

To segment the subcortical structures, FMRIB's Integrated Registration and Segmentation Tool (FIRST) v5.0.9 (www.fmrib.ox.ac.uk/fsl/, Oxford Centre for Functional MRI of the Brain) was used. FIRST is an automated model-based tool that runs a two-stage affine transformation to MNI152 space, to achieve a robust pre-alignment of thalamus, caudate nucleus, putamen, globus pallidus, hippocampus, amygdala, and nucleus accumbens based on individual’s T1-weighted MR images. Subcortical structures are modelled within a Bayesian framework (using manually segmented images provided by the Centre for Morphometric Analysis, CMA, MGH, Boston, as a prior) as surface meshes (masks) that were then fit to the registered image. Regions outside of the masks were excluded from subcortical alignment (68).

466 To assess hemispheric laterality for each subcortical structure, we calculated the Lateralization
467 Volume indices (LVs):

468 $$LV_s = \frac{V_{s_{right}} - V_{s_{left}}}{V_{s_{right}} + V_{s_{left}}} \qquad \text{Equation 1}$$

469 Where $V_{s_{right}}$ and $V_{s_{left}}$ represent the anatomical volume of a given subcortical structure (s) in
470 number of voxels, in the right and left hemisphere, respectively. This equation implicitly
471 controls for individual differences in brain volumes and has been commonly used to compute
472 hemispheric structural asymmetries (Mazzetti et al., 2019). LVs can range between -1 and 1
473 where a positive LV indicates rightward asymmetry and vice versa.

474 MEG data acquisition

475 Electromagnetic data were recorded from participants while seated in upright position, using a
476 306-sensor whole-head TRIUX system from MEGIN (MEGIN, Stockholm, Sweden) including 102
477 magnetometers and 204 (2x102 orthogonal) planar gradiometers. The MEG data were sampled
478 at 1000Hz, following an embedded anti-aliasing low-pass filter at 330 Hz and stored for offline
479 analysis. Head position of the participants was monitored by coils placed on anatomical
480 fiducials (nasion, left and right periauricular points), digitized using a Polhemus Fastrack
481 electromagnetic digitizer system (Polhemus Inc.). Eye movements were recorded using an
482 Eyelink eyetracker (EyeLink 1000, SR research Ltd., Ottawa, Canada) along with vertical EOG
483 sensors.

484 MEG data analysis

485 MEG data analysis was performed using custom scripts in MATLAB 2017a and 2019b (The
486 MathWorks) and the FieldTrip toolbox (71). The analysis pipeline was adapted from the FLUX
487 pipeline (72) and the scripts are available at https://github.com/tghafari/AMI_Substructures.

Preprocessing

Raw MEG data were high-pass filtered at 1Hz and demeaned. Then data were segmented in 4s epochs (-3s to 1s) relative to the target-onset (gaze shift of the face stimuli). Secondly, trials with sensors artifacts (e.g., jumps) were removed manually to prepare the data for automatic artifact attenuation using independent component analysis (ICA; "*runica.m*" in FieldTrip). Components related to eye blinks/movements, heartbeat and muscle activity were rejected. Thirdly, by visually inspecting the trials, we removed those containing clear residual artifacts such as eye blinks. We also removed trials with saccadic deviations larger than 3˚ from fixation (using EyeLink eye tracker data) during the 1.5s interval before target-onset (-1.5 – 0 s) (average ± SD = 13.7% ± 8.0 trials). Sensors that were removed during preprocessing were interpolated using a weighted neighbour estimate.

Time-frequency analysis of power

To calculate the time frequency representations (TFR) of power, we used a 3-cycle fixed time-window (e.g., 300ms for 10Hz) at each 10ms step. The data segments were multiplied by a Hanning taper to control the frequency smoothing and reduce spectral leakage. For computational efficiency, we also used a zero-padding, rounding up the length of segments to the next power of 2. Then a fast Fourier transform (FFT) was applied to the tapered segments in the 2-30 Hz frequency range in 1Hz steps and the power was estimated. The power was then summed for each gradiometer pair.

To quantify the anticipatory oscillatory activity, we focussed on the -850 to 0 ms interval before target onset. To select sensors constituting the region of interest (ROI), we calculated the 8-13 Hz alpha modulation index (MI(α)) for all sensors. TFR of power for each sensor was averaged over all trials in the -850 to 0 ms interval, for attention to right and left. Then the MI(α) for each participant and each sensor was calculated as:

$$MI(\alpha)_k = \frac{Power(\alpha)_{k_{att\ right}} - Power(\alpha)_{k_{att\ left}}}{Power(\alpha)_{k_{att\ right}} + Power(\alpha)_{k_{att\ left}}} \qquad \text{Equation 2}$$

Where Power(α)$_k$ denotes the alpha power at sensor *k* in each condition.

Subsequently, at the group level, MI(α) for all sensors on the left hemisphere were subtracted from the corresponding sensors on the right hemisphere. The resulting values were then sorted and five pairs of sensors (n_{ROI}) that showed the highest difference in MI(a) values were selected, resulting in 10 sensors, symmetrically distributed over the right and left hemispheres. Ten sensors were selected to ensure sufficient coverage of the region exhibiting alpha modulation as judged from prior work (62). As MI(α) consistently represents power of alpha in attention right versus attention left conditions, it entails the comparison between ipsilateral and contralateral alpha modulation power for sensors located on the right side of the head. The same comparison applies inversely for sensors situated on the left side of the brain.

To evaluate hemisphere-specific lateralization of alpha band modulation, we applied the hemispheric lateralization modulation (HLM(α)) index:

$$HLM(\alpha) = \frac{1}{n_{ROI}} \sum_{k=1}^{n_{ROI}} MI(\alpha)_{k_{right}} + \frac{1}{n_{ROI}} \sum_{k=1}^{n_{ROI}} MI(\alpha)_{k_{left}} \qquad \text{Equation 3}$$

Where n_{ROI} = 5 represents the number of sensors in each ROI and $MI(\alpha)_{k_{right}}$ or $MI(\alpha)_{k_{left}}$ denote the modulation index for sensor *k* over the right or left hemisphere, respectively.

530 We computed the modulation index (MI) for rapid invisible frequency tagging (RIFT) by
531 averaging the power of the signal in sensors on the right when attention was directed to the
532 right compared to when it was directed to the left. This calculation was also performed for
533 sensors on the left. Consequently, we identified the top 5 sensors on each side with the highest
534 MI as the Region of Interest (ROI). Utilizing the sensors within the ROI, we computed
535 hemispheric lateralization modulation (HLM) of RIFT by summing the average MI(RIFT) of the
536 right sensors and the average MI(RIFT) of the left sensors, obtaining one HLM(RIFT) value for
537 each participant. For a more comprehensive analysis, refer to reference (24).

538 Statistical analysis

539 *Generalized Linear Model*

540 To model how the mean expected value of HLM(α) indices depends on the lateralized volume
541 of subcortical structures, we applied a generalized linear model (GLM) using HLM(α) values as
542 the dependent variable and LV indices of subcortical structures as the systematic (explanatory)
543 variables. We performed a collinearity analysis (*vif.m* function in MATLAB) to ensure that the
544 predictor variables were sufficiently independent prior to performing the GLM analysis.

545 First, we sought to determine the best set of regressors that predicted variability in HLM(α)
546 values. We therefore used all possible combinations of regressors (LVs; one to seven
547 combinations) in a linear mixed-effects model (*fitme.m* function in MATLAB) to predict HLM(a)
548 indices and selected the model that scored the lowest using the Akaike information criterion
549 (AIC; (73)) score as the winning model. We confirmed our findings using Bayesian information
550 criterion (BIC; (74)) and produced similar results. These values are commonly used to identify
551 the best point of trade-off between fit and model complexity.

552 To estimate the beta weights of the winning model the optimal set of regressors (here LV_{Th},
553 LV_{CN} and LV_{GP}) were used as the explanatory variables in a GLM (*fitlm.m* function in MATLAB) to
554 predict HLM(a) values with the following formula:

555 $$HLM(\alpha) \sim \beta_0 + \beta_1 LV_{Th} + \beta_2 LV_{CN} + \beta_3 LV_{GP} + \varepsilon \qquad \text{Equation 4}$$

556 Here, LV_{Th}, LV_{CN} and LV_{GP} refer to the lateralization volume of thalamus, caudate nucleus, and
557 globus pallidus, respectively.

558 The absence of a relationship between modulations of alpha oscillations and the hippocampus
559 and amygdala was expected as these regions typically are not associated with the allocation of
560 spatial attention and thus add validity to our approach.

561 *Multivariate multiple regression*

562 To simultaneously model the predictive relationship between the lateralized volume of
563 thalamus, caudate, and globus pallidus, and all four load conditions, we used a multivariate
564 multiple regression (MMR) (75) analysis. MMR is used to predict multiple dependent variables
565 using multiple systematic parameters. It allows for modifying our hypothesis tests and
566 confidence intervals for explanatory parameters and responses, respectively (76). The model
567 was defined as:

568 $$HLM(\alpha_1) + HLM(\alpha_2) + HLM(\alpha_3) + HLM(\alpha_4) \sim \beta_0 + \beta_1 LV_{Th} + \beta_2 LV_{CN} + \beta_3 LV_{GP} + \varepsilon$$
569 Equation 5

570 Where HLM(α) refers to hemispheric lateralization modulation of alpha power in load
571 conditions 1 to 4 (Figure 1C), respectively; β refers to the coefficients in the model; LV_{Th}, LV_{CN}
572 and LV_{GP} refer to the lateralization volume of thalamus, caudate nucleus, and globus pallidus,
573 respectively.

574 To ensure our chosen MMR predicts meaningful variance in HLM(a) scores, we compared a full
575 model containing LV indexes from all 7 subcortical regions to one where the key structures of
576 interest (i.e., thalamus, caudate nucleus, and globus pallidus) had been removed, leaving
577 putamen, nucleus accumbens, hippocampus, and amygdala as regressors. This model is
578 referred to as the reduced model. We also compared a model containing the key regressors of

interest (LV_{Th}, LV_{CN}, LV_{GP}) to a null model that contained only subject intercepts as regressors. Models were compared one-way ANOVA test in RStudio (version 2022.02.0) (77).

To examine the specificity of each regressor for lateralized alpha in each condition, we statistically assessed the results of the MMR against the null hypothesis that a particular predictor does not contribute to all dependent variables, employing a MANOVA test in RStudio (version 2022.02.2) (77).

Behavioral data analysis

To evaluate if the participants response times and accuracy was correlated with the hemispheric lateralization of alpha oscillatory activity as well as lateralized volume of subcortical structures, we calculated behavioral asymmetry (BA) as below:

$$BA_{ACC/RT} = \frac{ACC/RT_{att\ right} - ACC/RT_{att\ left}}{ACC/RT_{att\ right} + ACC/RT_{att\ left}} \qquad \text{Equation 6}$$

Where $ACC/RT_{att\ right}$ and $ACC/RT_{att\ left}$ correspond to the behavioural asymmetric performance in accuracy or response times when the attention was toward right or left visual hemifield, respectively. Finally, we ran the winning GLM model with accuracy and response times as the dependent variable and LV_{Th}, LV_{CN}, and LV_{GP} as the regressors.

Acknowledgement

This work was funded by the Ministry of Defence, UK, through the mTBI Predict Consortium and supported by the NIHR Oxford Health Biomedical Research Centre (NIHR203316). The views expressed are those of the author(s) and not necessarily those of the NIHR or the Department of Health and Social Care.

The computations described in this paper were performed using the University of Birmingham's BlueBEAR HPC service, which provides a High Performance Computing service to the University's research community. See http://www.birmingham.ac.uk/bear for more details.

We express our gratitude to Jonathan L. Winter for assisting us with the MEG recordings.

Bibliography

1. Nobre AC, Kastner S. Oxford University Press, New York, NY, US. 2014 [cited 2022 Dec 20]. The Oxford handbook of attention. Oxford Library of Psychology. Available from: https://www.google.co.uk/books/edition/The_Oxford_Handbook_of_Attention/mtXQAgAAQBAJ?hl=en&gbpv=1&dq=the+oxford+handbook+of+attention&pg=PP1&printsec=frontcover

2. Desimone R. Neural Mechanisms of Selective Visual Attention. Annu Rev Neurosci. 1995;18(1):193–222.

3. Moran J, Desimone R. Selective attention gates visual processing in the extrastriate cortex. Science. 1985;229(4715):782–4.

4. Corbetta M, Shulman GL. Control of goal-directed and stimulus-driven attention in the brain. Nat Rev Neurosci. 2002;3(3):201–15.

5. Noudoost B, Chang MH, Steinmetz NA, Moore T. Top-down control of visual attention. Curr Opin Neurobiol. 2010 Apr 1;20(2):183–90.

6. Kastner S, Pinsk MA, De Weerd P, Desimone R, Ungerleider LG. Increased Activity in Human Visual Cortex during Directed Attention in the Absence of Visual Stimulation. Neuron. 1999 Apr 1;22(4):751–61.

7. Hopfinger JB, Buonocore MH, Mangun GR. The neural mechanisms of top-down attentional control. Nat Neurosci 2000 33. 2000 Mar;3(3):284–91.

8. Corbetta M, Kincade JM, Ollinger JM, Mcavoy MP, Shulman GL. Voluntary orienting is dissociated from target detection in human posterior parietal cortex. 2000 [cited 2023 Mar 2]; Available from: http://neurosci.nature.com

9. Kastner S, Fiebelkorn IC, Eradath MK. Dynamic pulvino-cortical interactions in the primate attention network. Curr Opin Neurobiol. 2020;65:10–9.

10. Krauzlis RJ, Lovejoy LP, Zénon A. Superior colliculus and visual spatial attention. Annu Rev Neurosci. 2013 Jul 8;36:165–82.

11. Krauzlis RJ, Bogadhi AR, Herman JP, Bollimunta A. Selective attention without a neocortex. Cortex. 2018 May 1;102:161–75.

12. Zhou H, Schafer RJ, Desimone R. Pulvinar-Cortex Interactions in Vision and Attention. Neuron. 2016 Jan 6;89(1):209–20.

13. Van Schouwenburg MR, Den Ouden HEM, Cools R. The Human Basal Ganglia Modulate Frontal-Posterior Connectivity during Attention Shifting. J Neurosci. 2010 Jul 21;30(29):9910–8.

14. Nakajima M, Schmitt LI, Halassa MM. Prefrontal Cortex Regulates Sensory Filtering through a Basal Ganglia-to-Thalamus Pathway. Neuron. 2019 Aug 7;103(3):445-458.e10.

15. Moolchand P, Jones SR, Frank MJ. Biophysical and Architectural Mechanisms of Subthalamic Theta under Response Conflict. J Neurosci Off J Soc Neurosci. 2022 Jun 1;42(22):4470–87.

16. Slagter HA, Mazaheri A, Reteig LC, Smolders R, Figee M, Mantione M, et al. Contributions of the ventral striatum to conscious perception: An intracranial EEG study of the attentional blink. J Neurosci. 2017 Feb 1;37(5):1081–9.

17. van Schouwenburg MR, den Ouden HEM, Cools R. Selective Attentional Enhancement and Inhibition of Fronto-Posterior Connectivity by the Basal Ganglia During Attention Switching. Cereb Cortex. 2015 Jun 1;25(6):1527–34.

18. Kelly SP, Lalor EC, Reilly RB, Foxe JJ. Increases in alpha oscillatory power reflect an active retinotopic mechanism for distracter suppression during sustained visuospatial attention. J Neurophysiol. 2006 Jun;95(6):3844–51.

19. Okazaki YO, De Weerd P, Haegens S, Jensen O. Hemispheric lateralization of posterior alpha reduces distracter interference during face matching. Brain Res. 2014 Nov 24;1590(1):56–64.

20. Thut G, Nietzel A, Brandt SA, Pascual-Leone A. α-Band electroencephalographic activity over occipital cortex indexes visuospatial attention bias and predicts visual target detection. J Neurosci [Internet]. 2006 Sep [cited 2023 Feb 17];26(37). Available from: https://www.jneurosci.org/content/26/37/9494

21. Worden MS, Foxe JJ, Wang N, Simpson GV. Anticipatory biasing of visuospatial attention indexed by retinotopically specific alpha-band electroencephalography increases over occipital cortex. J Neurosci Off J Soc Neurosci. 2000 Mar 15;20(6):RC63–RC63.

22. Jensen O. Gating by alpha band inhibition revised: a case for a secondary control mechanism [Internet]. PsyArXiv; 2023 Jan [cited 2023 Mar 23]. Available from: https://osf.io/7bk32

23. Lavie N. Perceptual load as a necessary condition for selective attention. J Exp Psychol Hum Percept Perform. 1995;21:451–68.

24. Gutteling TP, Sillekens L, Lavie N, Jensen O. Alpha oscillations reflect suppression of distractors with increased perceptual load. Prog Neurobiol. 2022 Jul 1;214:102285.

667 25. Mazzetti C, Staudigl T, Marshall TR, Zumer JM, Fallon SJ, Jensen O. Hemispheric Asymmetry
668 of Globus Pallidus Relates to Alpha Modulation in Reward-Related Attentional Tasks. J
669 Neurosci. 2019;39(46):9221–36.

670 26. Kasanova Z, Ceccarini J, Frank MJ, Amelsvoort T van, Booij J, Heinzel A, et al. Striatal
671 dopaminergic modulation of reinforcement learning predicts reward-oriented behavior in
672 daily life. Biol Psychol. 2017 Jul;127:1–9.

673 27. Cools R, Frank MJ, Gibbs SE, Miyakawa A, Jagust W, D'Esposito M. Striatal Dopamine
674 Predicts Outcome-Specific Reversal Learning and Its Sensitivity to Dopaminergic Drug
675 Administration. J Neurosci. 2009 Feb 4;29(5):1538–43.

676 28. Hikosaka O, Kim HF, Yasuda M, Yamamoto S. Basal Ganglia Circuits for Reward Value–
677 Guided Behavior. Annu Rev Neurosci. 2014;37(1):289–306.

678 29. Fallon SJ, Cools R. Reward acts on the pFC to enhance distractor resistance of working
679 memory representations. J Cogn Neurosci. 2014 Dec;26(12):2812–26.

680 30. Montague PR, Hyman SE, Cohen JD. Computational roles for dopamine in behavioural
681 control. Nature. 2004 Oct;431(7010):760–7.

682 31. Alberto GE, Stapleton-Kotloski JR, Klorig DC, Rogers ER, Constantinidis C, Daunais JB, et al.
683 MEG source imaging detects optogenetically-induced activity in cortical and subcortical
684 networks. 2021;12(1):1–13.

685 32. Griffiths BJ, Martín-Buro MC, Staresina BP, Hanslmayr S. Disentangling neocortical
686 alpha/beta and hippocampal theta/gamma oscillations in human episodic memory
687 formation. NeuroImage. 2021 Nov 15;242:118454.

688 33. Meyer SS, Rossiter H, Brookes MJ, Woolrich MW, Bestmann S, Barnes GR. Using generative
689 models to make probabilistic statements about hippocampal engagement in MEG.
690 NeuroImage. 2017 Apr 1;149:468–82.

691 34. Ruzich E, Crespo-García M, Dalal SS, Schneiderman JF. Characterizing hippocampal
692 dynamics with MEG: A systematic review and evidence-based guidelines. Hum Brain Mapp.
693 2019 Mar;40(4):1353–75.

694 35. Baillet S. Magnetoencephalography for brain electrophysiology and imaging. Nat Neurosci.
695 2017 Feb 23;20(3):327–39.

696 36. Shigeto H, Morioka T, Hisada K, Nishio S, Ishibashi H, Kira DI, et al. Feasibility and limitations
697 of magnetoencephalographic detection of epileptic discharges: Simultaneous recording of
698 magnetic fields and electrocorticography. Neurol Res. 2002 Sep 1;24(6):531–6.

37. Maguire EA, Gadian DG, Johnsrude IS, Good CD, Ashburner J, Frackowiak RSJ, et al. Navigation-related structural change in the hippocampi of taxi drivers. Proc Natl Acad Sci. 2000 Apr 11;97(8):4398–403.

38. Mak E, Bergsland N, Dwyer MG, Zivadinov R, Kandiah N. Subcortical Atrophy Is Associated with Cognitive Impairment in Mild Parkinson Disease: A Combined Investigation of Volumetric Changes, Cortical Thickness, and Vertex-Based Shape Analysis. Am J Neuroamerican J Neuro [Internet]. 2014 [cited 2023 Feb 27]; Available from: http://dx.doi.org/10.3174/ajnr.A4055

39. Yi HA, Möller C, Dieleman N, Bouwman FH, Barkhof F, Scheltens P, et al. Relation between subcortical grey matter atrophy and conversion from mild cognitive impairment to Alzheimer's disease. J Neurol Neurosurg Psychiatry. 2016 Apr 1;87(4):425–32.

40. Ye R, O'Callaghan C, Rua C, Hezemans FH, Holland N, Malpetti M, et al. Locus Coeruleus Integrity from 7 T MRI Relates to Apathy and Cognition in Parkinsonian Disorders. Mov Disord. 2022;37(8):1663–72.

41. Aylward EH, Codori AM, Rosenblatt A, Sherr M, Brandt J, Stine OC, et al. Rate of caudate atrophy in presymptomatic and symptomatic stages of Huntington's disease. Mov Disord. 2000;15(3):552–60.

42. Jafari Z, Kolb BE, Mohajerani MH. Neural oscillations and brain stimulation in Alzheimer's disease. Prog Neurobiol. 2020 Nov;194:101878.

43. Jenkinson N, Brown P. New insights into the relationship between dopamine, beta oscillations and motor function. Trends Neurosci. 2011 Dec;34(12):611–8.

44. Kong XZ, Mathias SR, Guadalupe T, ENIGMA Laterality Working Group, Glahn DC, Franke B, et al. Mapping cortical brain asymmetry in 17,141 healthy individuals worldwide via the ENIGMA Consortium. Proc Natl Acad Sci [Internet]. 2018 May 29 [cited 2023 Nov 23];115(22). Available from: https://pnas.org/doi/full/10.1073/pnas.1718418115

45. Minkova L, Habich A, Peter J, Kaller CP, Eickhoff SB, Klöppel S. Gray matter asymmetries in aging and neurodegeneration: A review and meta-analysis. Hum Brain Mapp. 2017 Dec;38(12):5890–904.

46. Roe JM, Vidal-Piñeiro D, Sørensen Ø, Brandmaier AM, Düzel S, Gonzalez HA, et al. Asymmetric thinning of the cerebral cortex across the adult lifespan is accelerated in Alzheimer's disease. Nat Commun. 2021 Feb 1;12(1):721.

47. Saalmann YB, Pinsk MA, Wang L, Li X, Kastner S. The pulvinar regulates information transmission between cortical areas based on attention demands. Science. 2012 Aug 10;337(6095):753–6.

733 48. Bogadhi AR, Bollimunta A, Leopold DA, Krauzlis RJ. Brain regions modulated during covert
734 visual attention in the macaque. Sci Rep. 2018 Oct 15;8(1):1–15.

735 49. Green JJ, Boehler CN, Roberts KC, Chen LC, Krebs RM, Song AW, et al. Cortical and
736 subcortical coordination of visual spatial attention revealed by simultaneous EEG-fMRI
737 recording. J Neurosci. 2017;37(33):7803–10.

738 50. Petersen SE, Robinson DL, Morris JD. Contributions of the pulvinar to visual spatial
739 attention. Neuropsychologia. 1987 Jan 1;25:97–105.

740 51. Abbasi O, Hirschmann J, Storzer L, Özkurt TE, Elben S, Vesper J, et al. Unilateral deep brain
741 stimulation suppresses alpha and beta oscillations in sensorimotor cortices. NeuroImage.
742 2018 Jul 1;174:201–7.

743 52. McFarland NR, Haber SN. Thalamic relay nuclei of the basal ganglia form both reciprocal
744 and nonreciprocal cortical connections, linking multiple frontal cortical areas. J Neurosci Off
745 J Soc Neurosci. 2002 Sep 15;22(18):8117–32.

746 53. Jeon HA, Anwander A, Friederici AD. Functional network mirrored in the prefrontal cortex,
747 caudate nucleus, and thalamus: High-resolution functional imaging and structural
748 connectivity. J Neurosci. 2014 Jul 9;34(28):9202–12.

749 54. Lanciego JL, Luquin N, Obeso JA. Functional Neuroanatomy of the Basal Ganglia. Cold Spring
750 Harb Perspect Med. 2012 Dec 1;2(12):a009621.

751 55. Chatham CH, Frank MJ, Badre D. Corticostriatal output gating during selection from working
752 memory. Neuron. 2014 Feb 19;81(4):930–42.

753 56. Crompe B de la, Aristieta A, Leblois A, Elsherbiny S, Boraud T, Mallet NP. The globus pallidus
754 orchestrates abnormal network dynamics in a model of Parkinsonism. Nat Commun. 2020
755 Dec 1;11(1):1–14.

756 57. Goldberg JH, Farries MA, Fee MS. Basal ganglia output to the thalamus: still a paradox.
757 Trends Neurosci. 2013 Dec 1;36(12):695–705.

758 58. Marshall TR, Bergmann TO, Jensen O. Frontoparietal Structural Connectivity Mediates the
759 Top-Down Control of Neuronal Synchronization Associated with Selective Attention. PLoS
760 Biol. 2015;

761 59. D'Andrea A, Chella F, Marshall TR, Pizzella V, Romani GL, Jensen O, et al. Alpha and alpha-
762 beta phase synchronization mediate the recruitment of the visuospatial attention network
763 through the Superior Longitudinal Fasciculus. NeuroImage. 2019 Mar 1;188(March
764 2018):722–32.

60. Ghafari T, Jounghani AR, Esteky H. Where and when matter in visual recognition. Atten Percept Psychophys. 2022;

61. Buxbaum LJ, Ferraro MK, Veramonti T, Farne A, Whyte J, Ladavas E, et al. Hemispatial neglect: Subtypes, neuroanatomy, and disability. Neurology. 2004 Mar 9;62(5):749–56.

62. Zhigalov A, Herring JD, Herpers J, Bergmann TO, Jensen O. Probing cortical excitability using rapid frequency tagging. NeuroImage. 2019;195(December 2018):59–66.

63. Jiji S, Smitha KA, Gupta AK, Pillai VPM, Jayasree RS. Segmentation and volumetric analysis of the caudate nucleus in Alzheimer's disease. Eur J Radiol. 2013 Sep 1;82(9):1525–30.

64. Sauseng P, Klimesch W, Heise KF, Gruber WR, Holz E, Karim AA, et al. Brain Oscillatory Substrates of Visual Short-Term Memory Capacity. Curr Biol. 2009;19(21):1846–52.

65. Wang XD, Wang M, Chen L. Hemispheric lateralization for early auditory processing of lexical tones: Dependence on pitch level and pitch contour. Neuropsychologia. 2013 Sep 1;51(11):2238–44.

66. Brainard DH. The Psychophysics Toolbox. Spat Vis. 1997;

67. Pelli GD. The VideoToolbox software for visual psychophysics: transforming numbers into movies. Spat Vis. 1997;10(4):437–42.

68. Patenaude B, Smith SM, Kennedy DN, Jenkinson M. A Bayesian model of shape and appearance for subcortical brain segmentation. NeuroImage. 2011 Jun 1;56(3):907–22.

69. Guadalupe T, Mathias SR, vanErp TGMM, Whelan CD, Zwiers MP, Abe Y, et al. Human subcortical brain asymmetries in 15,847 people worldwide reveal effects of age and sex. Brain Imaging Behav 2016 115. 2016 Oct 13;11(5):1497–514.

70. Okada N, Fukunaga M, Yamashita F, Koshiyama D, Yamamori H, Ohi K, et al. Abnormal asymmetries in subcortical brain volume in schizophrenia. Mol Psychiatry. 2016 Jan 19;21(10):1460–6.

71. Oostenveld R, Fries P, Maris E, Schoffelen JM. FieldTrip: Open source software for advanced analysis of MEG, EEG, and invasive electrophysiological data. Comput Intell Neurosci. 2011;2011.

72. Ferrante O, Liu L, Minarik T, Gorska U, Ghafari T, Luo H, et al. FLUX: A pipeline for MEG analysis. NeuroImage. 2022 Jun 1;253:119047.

73. Akaike H. A New Look at the Statistical Model Identification. IEEE Trans Autom Control. 1974;19(6):716–23.

74. Schwarz G. Estimating the Dimension of a Model. Ann Stat. 1978;6(2):461–4.

75. Manly BFJ, Alberto JAN. Multivariate Statistical Methods: A Primer, Fourth Edition. 4th ed. New York: Chapman and Hall/CRC; 2016. 269 p.

76. Dattalo P. Multivariate Multiple Regression. Anal Mult Depend Var. 2013 May 31;87–108.

77. R Core Team. R: A language and environment for statistical computing. R Foundation for Statistical Computing, Vienna, Austria | CiNii Research. 2020.

Modulation of alpha oscillations by attention is predicted by hemispheric asymmetry of subcortical regions.

Tara Ghafari[1], Cecilia Mazzetti[1], Kelly Garner[2], Tjerk Gutteling[1,3], Ole Jensen[1]
[1]Centre for Human Brain Health, School of Psychology, University of Birmingham, UK; [2]School of Psychology, University of New South Wales, Australia. [3]CERMEP-Imagerie du Vivant, MEG Department, Lyon, France

Supplementary materials

Table 1. Akaike Information Criterion (AIC) and Bayesian Information Criterion (BIC) values for all possible combinations of regressors (Lateralized Volume of subcortical structures). The selected model, with lowest AIC, is marked in green.

Regression	**Comb. 1**	**Comb. 2**	**Comb. 3**	**Comb. 4**	**Comb. 5**	**Comb. 6**	**Comb. 7**	**Comb. 8**	**Comb. 9**	**Comb. 10**	**Comb. 11**	**Comb. 12**	**Comb. 13**	**Comb. 14**	**Comb. 15**	**Comb. 16**	**Comb. 17**	**Comb. 18**	**Comb. 19**	**Comb. 20**	**Comb. 21**	**Model criterion**
$HLM \sim \beta_0$	-81.63	-77.78	-73.75	-78.62	-71.94	-73.18	-71.48	NaN	NaN	NaN	NaN	NaN	NaN	NaN	NaN	NaN	NaN	NaN	NaN	NaN	NaN	**AIC**
β_{LV_1}	-77.33	-73.48	-69.45	-74.32	-67.64	-68.88	-67.18	NaN	NaN	NaN	NaN	NaN	NaN	NaN	NaN	NaN	NaN	NaN	NaN	NaN	NaN	**BIC**
$HLM \sim \beta_0$	-86.72	-79.93	-82.66	-77.88	-78.04	-78.00	-76.42	-81.27	-75.82	-75.83	-73.89	-77.41	-70.41	-71.36	-69.94	-74.79	-76.05	-74.63	-70.08	-68.23	-69.30	**AIC**
$\beta_{LV_1} + \beta_{LV_2}$	-81.11	-74.32	-77.05	-72.28	-72.44	-72.39	-70.82	-75.66	-70.22	-70.23	-68.29	-71.81	-64.81	-65.75	-64.33	-69.19	-70.44	-69.03	-64.48	-62.63	-63.70	**BIC**
$HLM \sim \beta_0$	-85.30	-87.54	-82.79	-82.96	-82.64	-81.00	-76.18	-76.19	-76.29	-78.86	-79.00	-78.73	-74.25	-74.24	-74.32	-79.67	-74.61	-74.06	-72.55	-78.51	-78.88	**AIC**
$\beta_{LV_1} + \beta_{LV_2} + \beta_{LV_3}$	-78.46	-80.71	-75.95	-75.13	-75.81	-74.17	-69.34	-69.35	-69.46	-72.02	-72.17	-71.90	-67.42	-57.40	-67.49	-72.84	-67.77	-67.22	-65.72	-71.68	-72.05	**BIC**
$HLM \sim \beta_0$	-85.52	-81.42	-81.27	-81.21	-83.50	-83.73	-83.30	-79.33	-78.80	-78.85	-77.26	-77.72	-77.09	-72.43	-72.54	-72.49	-75.15	-74.95	-75.04	-70.57	-76.78	**AIC**
$\beta_{LV_1} + \beta_{LV_2} + \beta_{LV_3} + \beta_{LV_4}$	-77.52	-73.43	-73.28	-73.21	-75.50	-75.74	-75.31	-71.33	-70.80	-70.86	-69.27	-69.73	-69.10	-64.44	-64.55	-64.45	-67.15	-66.96	-67.04	-62.58	-68.78	**BIC**
$HLM \sim \beta_0$	-81.51	-81.90	-81.30	-77.65	-77.41	-77.17	-79.95	-79.32	-79.49	-75.29	-73.88	-73.36	-73.75	-68.77	-71.22	-75.31	-72.78	-73.87	-68.85	-72.63	-67.74	**AIC**
$\beta_{LV_1} + \beta_{LV_2} + \beta_{LV_3} + \beta_{LV_4} + \beta_{LV_5}$	-72.44	-72.83	-72.24	-68.58	-68.34	-68.01	-70.88	-70.25	-70.42	-66.22	-64.81	-64.29	-64.68	-59.70	-62.15	-66.24	-63.71	-64.79	-59.78	-63.56	-58.67	**BIC**
$HLM \sim \beta_0$	-78.13	-77.37	-77.70	-73.63	-75.76	-69.96	-71.25	NaN	NaN	NaN	NaN	NaN	NaN	NaN	NaN	NaN	NaN	NaN	NaN	NaN	NaN	**AIC**
$\beta_{LV_1} +$																						

$\beta_{LV_2} + \beta_{LV_3} + \beta_{LV_4} + \beta_{LV_5} + \beta_{LV_6}$	-68.07	-67.30	-67.63	-63.56	-65.70	-59.89	-61.19	NaN	NaN	NaN	NaN	NaN	NaN	NaN	NaN	NaN	NaN	NaN	NaN	NaN	NaN	**BIC**
$HLM \sim \beta_0$	-74.00	NaN	NaN	NaN	NaN	NaN	NaN	NaN	NaN	NaN	NaN	NaN	NaN	NaN	NaN	NaN	NaN	NaN	NaN	NaN	NaN	**AIC**
$\beta_{LV_1} + \beta_{LV_2} + \beta_{LV_3} + \beta_{LV_4} + \beta_{LV_5} + \beta_{LV_6} + \beta_{LV_7}$	-63.01	NaN	NaN	NaN	NaN	NaN	NaN	NaN	NaN	NaN	NaN	NaN	NaN	NaN	NaN	NaN	NaN	NaN	NaN	NaN	NaN	**BIC**

816

Regression	**Comb. 22**	**Comb. 23**	**Comb. 24**	**Comb. 25**	**Comb. 26**	**Comb. 27**	**Comb. 28**	**Comb. 29**	**Comb. 30**	**Comb. 31**	**Comb. 32**	**Comb. 33**	**Comb. 34**	**Comb. 35**	**Model criterion**
$HLM \sim \beta$ β_{LV_1}	NaN	NaN	NaN	NaN	NaN	NaN	NaN	NaN	NaN	NaN	NaN	NaN	NaN	NaN	**AIC**
	NaN	NaN	NaN	NaN	NaN	NaN	NaN	NaN	NaN	NaN	NaN	NaN	NaN	NaN	**BIC**
$HLM \sim \beta$ $\beta_{LV_1} + \beta_{LV_2}$	NaN	NaN	NaN	NaN	NaN	NaN	NaN	NaN	NaN	NaN	NaN	NaN	NaN	NaN	**AIC**
	NaN	NaN	NaN	NaN	NaN	NaN	NaN	NaN	NaN	NaN	NaN	NaN	NaN	NaN	**BIC**
$HLM \sim \beta$ $\beta_{LV_1} + \beta_{LV_2} + \beta_{LV_3}$	-77.34	-74.59	-71.90	-71.93	-73.54	-75.43	-73.45	-68.27	-66.72	-67.51	-72.40	-70.89	-72.05	-66.31	**AIC**
	-70.50	-67.75	-65.07	-65.09	-66.71	-68.59	-66.61	-61.43	-59.89	-60.67	-65.57	-64.05	-65.21	-59.48	**BIC**
$HLM \sim \beta$ $\beta_{LV_1} + \beta_{LV_2} + \beta_{LV_3} + \beta_{LV_4}$	-77.76	-75.76	-72.83	-70.69	-70.19	-76.72	-74.48	-74.97	-70.58	-71.67	-69.66	-71.44	-64.53	-68.46	**AIC**
	-69.76	-67.77	-64.84	-62.70	-62.19	-68.73	-66.49	-66.98	-62.59	-63.68	-61.67	-63.44	-56.53	-60.47	**BIC**
$HLM \sim \beta$ $\beta_{LV_1} + \beta_{LV_2} + \beta_{LV_3} + \beta_{LV_4} + \beta_{LV_5}$	NaN	NaN	NaN	NaN	NaN	NaN	NaN	NaN	NaN	NaN	NaN	NaN	NaN	NaN	**AIC**
	NaN	NaN	NaN	NaN	NaN	NaN	NaN	NaN	NaN	NaN	NaN	NaN	NaN	NaN	**BIC**
$HLM \sim \beta$ $\beta_{LV_1} + \beta_{LV_2} + \beta_{LV_3} + \beta_{LV_4} + \beta_{LV_5} + \beta_{LV_6}$	NaN	NaN	NaN	NaN	NaN	NaN	NaN	NaN	NaN	NaN	NaN	NaN	NaN	NaN	**AIC**
	NaN	NaN	NaN	NaN	NaN	NaN	NaN	NaN	NaN	NaN	NaN	NaN	NaN	NaN	**BIC**
$HLM \sim \beta$ $\beta_{LV_1} + \beta_{LV_2} + \beta_{LV_3} + \beta_{LV_4} + \beta_{LV_5} + \beta_{LV_6} + \beta_{LV_7}$	NaN	NaN	NaN	NaN	NaN	NaN	NaN	NaN	NaN	NaN	NaN	NaN	NaN	NaN	**AIC**
	NaN	NaN	NaN	NaN	NaN	NaN	NaN	NaN	NaN	NaN	NaN	NaN	NaN	NaN	**BIC**

Table 2. The combination of structures for each regression model above. The selected model is marked in green.

Regression	Comb. 1	Comb. 2	Comb. 3	Comb. 4	Comb. 5	Comb. 6	Comb. 7	Comb. 8	Comb. 9	Comb. 10	Comb. 11	Comb. 12	Comb. 13	Comb. 14	Comb. 15	Comb. 16	Comb. 17	Comb. 18	Comb. 19	Comb. 20	Comb. 21
$HLM \sim \beta_0$ β_{LV_1}	Th	CN	Put.	GP	Hipp.	Amyg.	Acc.														
$HLM \sim \beta_0$ $\beta_{LV_1} + \beta_{LV_2}$	Th + CN	Th + Put.	Th + GP	Th + Hipp.	Th + Amyg.	Th + Acc.	CN + Put.	CN + GP	CN + Hipp.	CN + Amyg.	CN + Acc.	Put. + GP	Put. + Hipp.	Put. + Amyg.	Put. + Acc.	GP + Hipp.	GP + Amyg.	GP + Acc.	Hipp. + Amyg.	Hipp. + Acc.	Amyg. + Acc.
$HLM \sim \beta_0$ $\beta_{LV_1} + \beta_{LV_2} + \beta_{LV_3}$	Th + CN + Put.	Th + CN + GP	Th + CN + Hipp.	Th + CN + Amyg.	Th + CN + Acc.	Th + Put. + GP	Th + Put. + Hipp.	Th + Put. + Amyg.	Th + Put. + Acc.	Th + GP + Hipp.	Th + GP + Amyg.	Th + GP + Acc.	Th + Hipp. + Amyg.	Th + Hipp. + Acc.	Th + Amyg. + Acc.	CN + Put. + GP	CN + Put. + Hipp.	CN + Put. + Amyg.	CN + Put. + Acc.	CN + GP + Hipp.	CN + GP + Amyg.
$HLM \sim \beta_0$ $\beta_{LV_1} + \beta_{LV_2} + \beta_{LV_3} + \beta_{LV_4}$	Th + CN + Put. + GP	Th + CN + Put. + Hipp.	Th + CN + Put. + Amyg.	Th + CN + Put. + Acc.	Th + CN + GP + Hipp.	Th + CN + GP + Amyg.	Th + CN + GP + Acc.	Th + CN + Hipp. + Amyg.	Th + CN + Hipp. + Acc.	Th + CN + Amyg. + Acc.	Th + Put. + GP + Hipp.	Th + Put. + GP + Amyg.	Th + Put. + GP + Acc.	Th + Put. + Hipp. + Amyg.	Th + Put. + Hipp. + Acc.	Th + Put + Amyg. + Acc.	Th + GP + Hipp. + Amyg.	Th + GP + Hipp. + Acc.	Th + GP + Amyg. + Acc.	Th + Hipp. + Amyg. + Acc.	CN + Put. + GP + Hipp.
$HLM \sim \beta_0$ $\beta_{LV_1} + \beta_{LV_2} + \beta_{LV_3} + \beta_{LV_4} + \beta_{LV_5}$	Th + CN + Put. + GP + Hipp.	Th + CN + Put. + GP + Amyg.	Th + CN + Put. + GP + Acc.	Th + CN + Put. + Hipp. + Amyg.	Th + CN + Put. + Hipp. + Acc.	Th + CN + Put. + Amyg. + Acc.	Th + CN + GP + Hipp. + Amyg.	Th + CN + GP + Hipp. + Acc.	Th + CN + GP + Amyg. + Acc.	Th + CN + Hipp. + Amyg. + Acc.	Th + Put. + GP + Hipp. + Amyg.	Th + Put. + GP + Hipp. + Acc.	Th + Put. + GP + Amyg. + Acc.	Th + Put. + Hipp. + Amyg. + Acc.	Th + GP + Hipp. + Amyg. + Acc.	CN + Put. + GP + Hipp. + Acc.	CN + Put. + GP + Hipp. + Amyg.	CN + Put. + GP + Amyg. + Acc.	CN + Put. + Hipp. + Amyg. + Acc.	CN + GP + Hipp. + Amyg. + Acc.	Put. + GP + Hipp. + Amyg. + Acc.
$HLM \sim \beta_0$ $\beta_{LV_1} + \beta_{LV_2} + \beta_{LV_3} + \beta_{LV_4} + \beta_{LV_5} + \beta_{LV_6}$	Th + CN + Put. + GP + Hi	Th + CN + Put. + GP + Hi	Th + CN + Put. + GP + A	Th + CN + Put. + Hipp. +	Th + CN + GP + Hipp. + A	Th + Put. + GP + Hipp. +	CN + Put. + GP + Hipp. +														

	pp. + Amyg.	pp. + Acc.	myg. + Acc.	Amyg. + Acc.	myg. + Acc.	Amyg. + Acc.	Amyg. + Acc.														
$HLM \sim \beta_0$ $\beta_{LV_1} +$ $\beta_{LV_2} +$ $\beta_{LV_3} +$ $\beta_{LV_4} +$ $\beta_{LV_5} +$ $\beta_{LV_6} +$ β_{LV_7}	Th + CN + Put. + GP + Hipp. + Amyg. + Acc.																				

820

Regression	**Comb. 22**	**Comb. 23**	**Comb. 24**	**Comb. 25**	**Comb. 26**	**Comb. 27**	**Comb. 28**	**Comb. 29**	**Comb. 30**	**Comb. 31**	**Comb. 32**	**Comb. 33**	**Comb. 34**	**Comb. 35**
$HLM \sim \beta$ β_{LV_1}	NaN	NaN	NaN	NaN	NaN	NaN	NaN	NaN	NaN	NaN	NaN	NaN	NaN	NaN
$HLM \sim \beta$ $\beta_{LV_1} +$ β_{LV_2}	NaN	NaN	NaN	NaN	NaN	NaN	NaN	NaN	NaN	NaN	NaN	NaN	NaN	NaN
$HLM \sim \beta$ $\beta_{LV_1} +$ $\beta_{LV_2} +$ β_{LV_3}	CN + GP + Acc.	CN + Hipp. + Amyg.	CN + Hipp. + Acc.	CN + Amyg. + Acc.	Put. + GP + Hipp.	Put. + GP + Amyg.	Put. + GP + Acc.	Put. + Hipp. + Amyg.	Put. + Hipp. + Acc.	Put. + Amyg. + Acc.	GP + Hipp. + Amyg.	GP + Hipp. + Acc.	GP + Amyg. + Acc.	Hipp. + Amyg. + Acc.
$HLM \sim \beta$ $\beta_{LV_1} +$ $\beta_{LV_2} +$ $\beta_{LV_3} +$ β_{LV_4}	CN + Put. + GP + Hipp.	CN + Put. + GP + Amyg.	CN + Put. + GP + Acc.	CN + Put. + Hipp. + Amyg.	CN + Put. + Amyg. + Acc.	CN + GP + Hipp. + Amyg.	CN + GP + Hipp. + Acc.	CN + GP + Amyg. + Acc.	CN + Hipp. + Amyg. + Acc.	Put. + GP + Hipp. + Amyg	Put. + GP + Hipp. + Acc.	Put. + GP + Amyg. + Acc.	Put. + Hipp. + Amyg. + Acc	GP + Hipp. + Amyg. + Acc.

$HLM \sim \beta$ $\beta_{LV_1} +$ $\beta_{LV_2} +$ $\beta_{LV_3} +$ $\beta_{LV_4} +$ β_{LV_5}	NaN	NaN	NaN	NaN	NaN	NaN	NaN	NaN	NaN	NaN	NaN	NaN	NaN	NaN
$HLM \sim \beta$ $\beta_{LV_1} +$ $\beta_{LV_2} +$ $\beta_{LV_3} +$ $\beta_{LV_4} +$ $\beta_{LV_5} +$ β_{LV_6}	NaN	NaN	NaN	NaN	NaN	NaN	NaN	NaN	NaN	NaN	NaN	NaN	NaN	NaN
$HLM \sim \beta$ $\beta_{LV_1} +$ $\beta_{LV_2} +$ $\beta_{LV_3} +$ $\beta_{LV_4} +$ $\beta_{LV_5} +$ $\beta_{LV_6} +$ β_{LV_7}	NaN	NaN	NaN	NaN	NaN	NaN	NaN	NaN	NaN	NaN	NaN	NaN	NaN	NaN

Figure 1. Lateralization volume of thalamus, caudate nucleus and globus pallidus in relation to hemispheric lateralization modulation of rapid invisible frequency tagging (HLM(RIFT)) on the right and behavioural asymmetry on the left. A and E, The beta coefficients for the best model (having three regressors) associated with a generalized linear model (GLM) where lateralization volume (LV) values were defined as explanatory variables for HLM(RIFT) (A) and behavioural asymmetry (E). Error bars indicate standard errors of mean (SEM). B and F, Partial regression plot showing the association between LV_{Th} and HLM(RIFT) (B, p-value = 0.59) and behavioural asymmetry (F, p-value = 0.38) while controlling for LV_{GP} and LV_{CN}. C and G, Partial regression plot showing the association between LV_{GP} and HLM(RIFT) (C, p-value = 0.16) and behavioural asymmetry (G, p-value = 0.80) while controlling for LV_{Th} and LV_{CN} . D and H, Partial regression plot showing the association between LV_{CN} and HLM(RIFT) (D, p-value = 0.53) and behavioural asymmetry (H, p-value = 0.74) while controlling for LV_{Th} and LV_{GP}. Negative (or positive) LVs indices denote greater left (or right) volume for a given substructure; similarly negative HLM(RIFT) values indicate stronger modulation of RIFT power in the left compared with the right hemisphere, and vice versa; positive behavioural asymmetry value shows higher accuracy when the target was on the right as compared with left, and vice versa for negative behavioural

840 asymmetry values. The dotted curves in B, C, D, F, G, and H indicate 95% confidence bounds for
841 the regression line fitted on the plot in red.

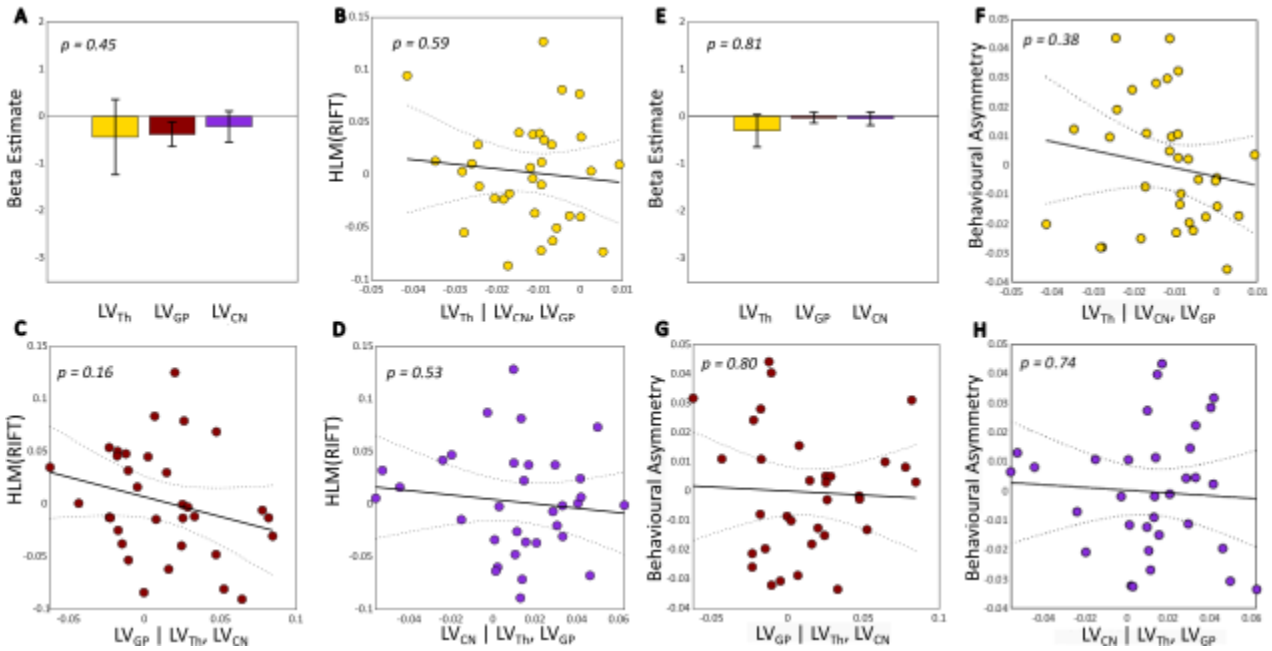

842
843
844
845 Table 3. Bayes factors for correlation between hemispheric laterality of subcortical structures
846 with hemispheric lateralization modulation of rapid invisible frequency tagging (HLM(RIFT)) and
847 with behavioural asymmetry (BA). The Pearson correlation between each subcortical structure
848 with HLM(RIFT) and behavioural asymmetry was calculated. The likelihood of the data under
849 the alternative hypothesis (the evidence of correlation) were subsequently compared to the
850 likelihood under null hypothesis (absence of correlation), given the data. As it is demonstrated
851 in the table, all Bayes factors were below or very close to 1 indicating evidence for the null
852 hypothesis.
853

Subcortical structure	**HLM(RIFT)**	**BA**
Thalamus	0.14	0.20
Caudate Nucleus	0.18	0.15
Putamen	0.14	0.14
Globus Pallidus	0.34	0.13
Hippocampus	0.19	0.25
Amygdala	0.54	1.18
Nucleus Accumbens	0.16	0.17

854